SUBSOLIDUS PHASE DIAGRAM OF BINARY SYSTEM IN THE PEROVSKITE TYPE LAYER COMPOUNDS $(n\text{-}C_nH_{2n+1}NH_3)_2MnCl_4$

K. Wu[*] and J. Zhang

Department of Chemistry and Material Science, Key Laboratory of Inorganic Nano-materials of Hebei Province
Hebei Normal University, 113 YuHua Rd. Shijiazhuang, 050016, China

The thermotropic phase transitions in the perovskite type layer compound $(n\text{-}C_{10}H_{21}NH_3)_2MnCl_4$ and $(n\text{-}C_{14}H_{29}NH_3)_2MnCl_4$ were synthesized and, at the same time, a series of their mixtures $C_{10}Mn$–$C_{14}Mn$ were prepared. The experimental binary phase diagram of $C_{10}Mn$–$C_{14}Mn$ was established by differential thermal analysis (DTA), IR and X-ray diffraction. In the phase diagram new material $(n\text{-}C_{10}H_{21}NH_3)(n\text{-}C_{14}H_{29}NH_3)MnCl_4$ and two eutectoid invariants were observed, two eutectic points temperatures are about 29.8 and 27.9°C. Contrasting other similar system, there are three noticeable solid solution ranges (α, β, γ) at the left and right boundary and middle of the phase diagram.

Introduction

The *bis(n-alkylammonium)* tetrahelometallates with the general formula $(C_nH_{2n+1}NH_3)_2MCl_4$ (M=Cu, Mn, Cd, Zn, Co, …, X=Cl, Br) (short notation; C_nM) are known to crystallize in a bidimensional structure of perovskite [1–3]. Recently C_nM have attracted considerable attention because of their physical properties, including ferro-, piezo- or pyroelectricity, ferri-, anti-ferro- or piezomagnetism and non-linear optical effects, and their technical application for electro- or magneto-optical devices [3–6]. Herein we synthesized two materials of the type $[NR_4]_2MnCl_4$ in *bis(n-alkyl-ammonium)* tetrachloromanganate(II) with the general formula $(n\text{-}C_{10}H_{21}NH_3)_2MnCl_4$ (short notation; $C_{10}Mn$) and $(n\text{-}C_{14}H_{29}NH_3)_2MnCl_4$ (short notation; $C_{14}Mn$). The two compounds are known to crystallize in a perovskite structure. The $MnCl_4^{2-}$ anions are sandwiched between double layers of *n*-alkylammonium cations. The layers are bound by van der Waals forces between $(CH_2)_nCH_3$ groups and by long-range Coulomb forces, and the octahedral cavities are occupied by the $-NH_3^+$ polar head of the *n*-alkylammonium cations which weak N–H...Cl hydrogen bonds with the halogens. The physical properties and structure of C_nMn [6–9] and C_nZn systems [8, 9] have been previously researched. The binary phase diagram for $C_{10}Zn$–$C_{12}Zn$ [9], $C_{10}Zn$–$C_{16}Zn$ [8, 10], $C_{12}Zn$–$C_{16}Zn$ [8, 10], $C_{12}Zn$–$C_{18}Zn$ [11], $C_{10}Co$–$C_{16}Co$ [10], $C_{12}Co$–$C_{16}Co$ [10, 12], $C_{12}Mn$–$C_{16}Mn$ [13, 14] were reported. Among them, the diagram of $C_{10}Zn$–$C_{16}Zn$ [10], $C_{12}Mn$–$C_{16}Mn$ [13], $C_{10}Co$–$C_{16}Co$ [10, 12], $C_{12}Co$–$C_{16}Co$ [10] compared with other show absolute immiscibility. Now, the binary phase diagram of $C_{10}Mn$–$C_{14}Mn$ is not known. In this paper the subsolidus binary phase diagram of $C_{10}Mn$–$C_{14}Mn$ was established by DTA, IR and X-ray diffraction (XRD).

Experimental

$MnCl_2$, concentrated HCl and absolute ethanol used were analytical grade. Decylamine (C.P.) was purchased from Fluka AG (Japan) Plant; Tetradecylamine was purchased from Beijing Chemical Plant.

Compounds of the type C_nMn were obtained as platelets by mixing hot absolute ethanol solutions of $MnCl_2$ and concentrated HCl and the corresponding alkylamine in a 1:2:2 molal ratio. The solutions were concentrated by boiling, then allowed to cool to the room temperature and filtered. The products were recrystallized twice from absolute ethanol. At last, put them into the vacuum desiccator for 8 h at about 80°C. $C_{10}Mn$, $C_{14}Mn$ were analyzed with an MT-3 CHN elemental analyzer (Japan). The results of elemental analysis are in mass%, elemental analyses calc. (%) for $C_{10}Mn$: C 46.78, H 8.19, N 5.46; Found: C 45.51, H 9.20, N 5.37. Anal. calc. (%) for $C_{14}Mn$: C 53.76, H 9.28, N 4.48; Found: C 55.18, H 10.42, N 4.53. The $C_{10}Mn$ and $C_{14}Mn$ were weighed exactly in desired proportion to prepare different mixed samples. The two components were dissolved in absolute ethanol. Then part of the solvent was evaporated.

---

[*]   Author for correspondence: wukzh688@163.com

Air-dry samples were put into a vacuum desiccator for 8 h at temperature about 80°C. The concentrations of all materials in binary system were expressed with $W_{C_{10}Mn}$ %.

The DTA curve was measured on a CDR-4P differential scanning calorimeter (DTA; Shanghai Scale Instrument Plant) at a different scanning rate of 5°C min^{-1} in a static atmosphere. Samples that are about 4.5 mg were sealed in aluminum crucibles. FTIR-8900 IR Spectrum Analyzer (made in Japan); PTD-3 IR Control Temperature Apparatus and Vertical Heater. X-ray diffraction patterns on compacted samples of the powders were taken by D/MAX-RA X-ray diffractometer (made in Japan) using CuK$_\alpha$ radiation (Ni filter) at a scanning rate of 2° min^{-1}. Voltage/electric current is 40 kV/100 mA.

Results and discussion

Thermal analysis

Figure 1 show the DTA curves of $C_{10}Mn$–$C_{14}Mn$ with different $W_{C_{10}Mn}$ %. The results of DTA experiments obtained with 'Shape factors method' [15] are listed in Table 1. All the materials C_nMn show solid–solid phase transition in the temperature range 25–70°C. These are always reproducible after heating and cooling cycles throughout the transition points. The data in Table 1 shows that the value of the transition temperature decreases with increasing $W_{C_{10}Mn}$ % in the range from 0 to 28.86%. Then, the phase transition temperature first rises to from 28.86 to 53.74%. The first eutectoid temperature (about 29.8°C) appears in the $W_{C_{10}Mn}$ % range of 25.52–44.11%. The second decrease was found from 53.74 to about 70.00%. With $W_{C_{10}Mn}$ % increasing gradually from about 70.00%, the phase transition temperature rises again. The second eutectoid temperature at about 27.9°C was found in the $W_{C_{10}Mn}$ % range of 64.44–86.53%. Table 1 reveals that the first eutectic temperature is not close to $W_{C_{10}Mn}$ %=0, nor does the second eutectic temperature end near $W_{C_{10}Mn}$ %=100%. The range of the first eutectic temperature does not end close to the beginning of the second eutectic temperature. It is clear that the values of phase transition temperature of the binary system $C_{10}Mn$–$C_{14}Mn$ in solid–solid phase transitions show a waving dependence on $W_{C_{10}Mn}$ %. The reason be sure that there are not only an intermediate $(n\text{-}C_{10}H_{21}NH_3)(n\text{-}C_{14}H_{29}NH_3)MnCl_4$ (short notation; $C_{10}C_{14}Mn$) but also three solid solution ranges exist at the left, right boundary and middle of the phase diagram of $C_{10}Mn$–$C_{14}Mn$.

Table 1 Solid–solid transition temperatures of the $C_{10}Mn$–$C_{14}Mn$ system with measured increasing temperature

$W_{C_{10}Mn}$ %	T_{e1}/°C	T_{e2}/°C	T_{s1}/°C	T_{s2}/°C
0($C_{14}Mn$)			63.3	
3.87			61.2	63.2
8.33			57.8	63.0
11.50			54.7	62.7
17.67			42.3	57.2
21.19			38.1	51.2
25.52	29.3			43.5
28.86	29.8			34.5
35.23	29.7			36.2
44.11	29.8			41.3
48.16			41.7	43.2
53.74			36.7	43.7
60.48			31.2	38.9
64.44		27.7		34.8
73.21		27.9		32.3
81.13		27.9		32.2
84.21		27.5		32.3
86.53		27.9		31.8
90.68			28.5	32.0
96.12			28.8	31.8
100($C_{10}Mn$)			31.1	

Note: T_e – eutectoid invariant; T_s – solid–solid transition temperature
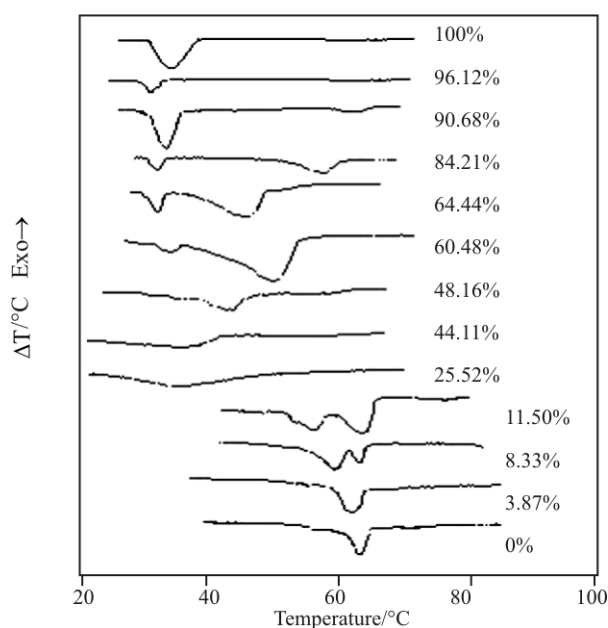

Fig. 1 DTA curves of $C_{10}Mn$–$C_{14}Mn$ with different $W_{C_{10}Mn}$ %

IR spectra at various temperatures

Figure 2 is IR spectra at various temperature and plot of wavenumber of absorption N–H bond *vs.* temperatures for 25.52% $C_{10}Mn$–$C_{14}Mn$. The leap of the temperature of the wavenumber coincides with the result of DTA.

The planar vibration of CH_2 comes forth with the scope of 850~700 cm^{-1}, it is sensitive to the piling structure of the molecule. Below the transition temperature, the planar vibration of CH_2 which is at 720 cm^{-1} has splits obviously, at room temperature they are at 721 and 719 cm^{-1} separately. When the temperature is raised, the absorption peak of N–H stretching vibration begins to move to the higher wavenumber, it is shown that the N–H…Cl hydrogen bonds weakened apparently. Accordingly, the degree of split of the planar vibration of CH_2 modified. All of these can give us such a conclusion: the main phase transition may due to the change of the piling structure. From the phase of the lower temperature to the phase of the higher temperature, the mutual function between the layers decrease distinctly and weak the hydrogen bonds, but there still have certain order to some degree.

At the higher temperature, there is a leap in the wavenumber of N–H stretching vibration. It is the result of the hydrogen bonds which had been weakened or even destroyed. Because of the weakening of the hydrogen bonds, a corresponding structural change occurs. The weakening of the N–H…Cl hydrogen bonds made the enchaining force to alkylammonium from the $MnCl_4^{2-}$ weakened and form another free disorder state–another kind of solid. The split of the factor group of the planar wagging vibration disappears. The raising of the temperature which made the high
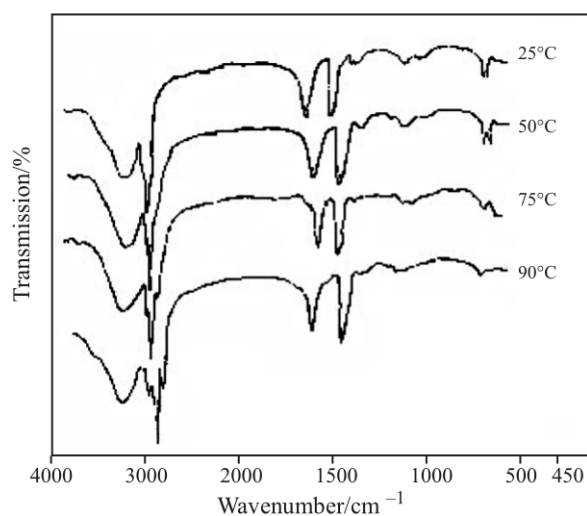
and low frequency move to the opposite direction separately is the reason. It demonstrates the reciprocal force between the chains decreased distinctly and an order–disorder change in the chains piling structure appeared.

The IR results of the other component of $C_{10}Mn$–$C_{14}Mn$ are in agreement with the data of the sample of 25.52%, the transition temperatures are near to the data of the DTA. This not only can reveal the solid–solid phase transition mechanism but can test the phase transition temperature. Therefore, it can be as the subsidiary method in drawing the phase diagram.

X-ray diffraction

Figure 3 show the diffraction patterns at room temperature for pure $C_{10}Mn$, $C_{14}Mn$ and their binary system. The diffraction patterns of sample with $W_{C_{10}Mn}$% of 3.87% has the similar to the pure $C_{14}Mn$, indicating a single-phase region. In this concentration range, $C_{10}C_{14}Mn$ dissolves in $C_{14}Mn$ to form a solid solution α. Similarly, samples with $W_{C_{10}Mn}$% from 96.12% to pure $C_{10}Mn$ have homologous patterns, revealing that $C_{10}C_{14}Mn$ dissolves in $C_{10}Mn$ to form a solid solution β. In the same way, samples $W_{C_{10}Mn}$% from 44.11 to 64.44% have similar diffraction patterns, showing that $C_{10}Mn$ or $C_{14}Mn$ dissolved in $C_{10}C_{14}Mn$, forming a single-phase γ. Samples with $W_{C_{10}Mn}$% from 25.52 to 44.11% are in the two-phase region, and their patterns are the overlap of α and γ. The patterns in $W_{C_{10}Mn}$%

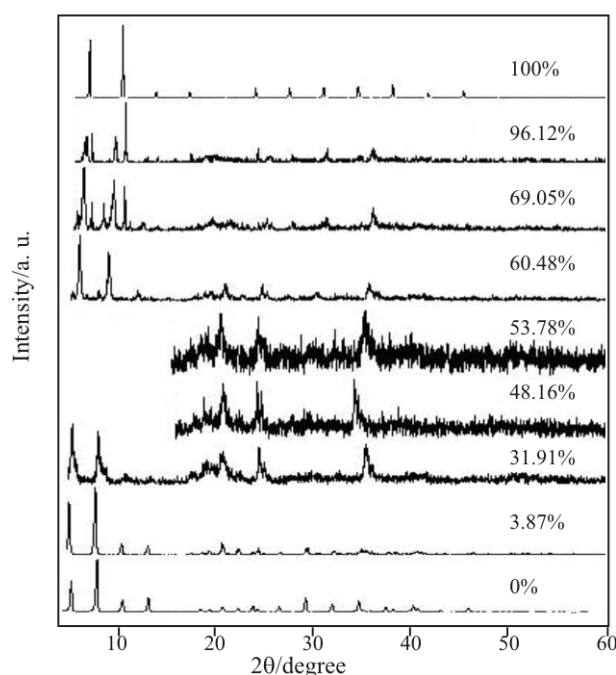**Fig. 2** IR spectra at various temperatures and plot of wavenumber of absorption N–H bond *vs.* temperatures for 25.52% $C_{10}Mn$–$C_{14}Mn$

Fig. 3 The diffraction patterns for $C_{10}Mn$, $C_{14}Mn$ and their binary system with different $W_{C_{10}Mn}$%

range of 64.44 to 86.53% are the overlap of β and γ and in the two-phase region. This above evidence that led us to strongly support the fact that the form of intermediate $(n\text{-}C_{10}H_{21}NH_3)(n\text{-}C_{14}H_{29}NH_3)MnCl_4$ and three solid solutions in the phase diagram of $C_{10}Mn–C_{14}Mn$.

Establishment of phase diagram

The binary phase diagram of $C_{10}Mn–C_{14}Mn$ (Fig. 4) was obtained according to the temperature-composition relations from the above DTA, IR and X-ray diffraction experiments. Figure 4 indicates that an intermediate compound $(n\text{-}C_{10}H_{21}NH_3)(n\text{-}C_{14}H_{29}NH_3)MnCl_4$ is formed, due to a top temperature between two eutectoid invariants [16–19]. The low temperature perovskite-layer structure of $C_{10}Mn$, $C_{14}Mn$ and their binary system are organized by neutralizing $MnCl_4^{2-}$ with alkylammonium ions. Alkylammonium chains are parallel to each other and slightly tilted with respect to the normal of the inorganic layers. The adjacent alkyl chains interact with each other by van der Waals interaction, and are hydrogen bonded to $MnCl_4^{2-}$. When the temperature is increased to 29.8°C, the first eutectoid invariant occurs from 25.52 to 44.11%. $C_{10}Mn$ and $C_{10}C_{14}Mn$ undergo a reversible solid–solid phase transformation. In this situation, the chains are in a large degree of motional freedom and a disordered phase appears. At the same time, the hydrogen bonds are weakened and even destroyed. The second eutectoid invariant appears from 64.44 to 86.53%, the temperature is 27.9°C. Similarly, $C_{14}Mn$ and $C_{10}C_{14}Mn$ undergo a reversible solid–solid phase transformation.

The binary phase diagram for a homologous system of $C_{10}Zn\text{-}C_{16}Zn$ [10], $C_{12}Mn–C_{16}Mn$ [15], $C_{10}Co–C_{16}Co$ [10, 12], $C_{12}Co–C_{16}Co$ [10] were

reported, the shape of which is similar to ours. The largest difference is that their diagram shows absolute immiscibility, while partial miscibility was observed in this work. As is well known, the phase diagram of binary systems is determined by the difference of two components. If their structure and size of two components are little different, they often dissolve each other and form miscible system. Conversely, when they are much difference, the degree of miscibility is limited. $C_{10}C_{14}Mn$ was considered that $C_{10}Mn$ and $C_{14}Mn$ has exchanged an alkylammonium chains by each other, so their structure and molecular size have little difference, which results in their partial miscibility.

Conclusions

The binary phase diagram of $(n\text{-}C_{10}H_{21}NH_3)_2MnCl_4$ and $(n\text{-}C_{14}H_{28}NH_3)_2MnCl_4$ mixtures was established by DTA, IR and XRD. A new material of $(n\text{-}C_{10}H_{21}NH_3)(n\text{-}C_{14}H_{29}NH_3)MnCl_4$ and two eutectoid invariants were observed. There are three noticeable solid solution ranges at the left boundary, right boundary, and middle of the phase diagram, respectively. The hydrogen bonds and van der Waals forces in the intermediate compound $(n\text{-}C_{10}H_{21}NH_3)(n\text{-}C_{14}H_{29}NH_3)MnCl_4$ and three solid solution ranges (α, β, γ) are stronger than that of other binary system, which are caused by the alkylammonium chains are an ordered phase in low degree of motional freedom. These results lead to the final transition temperature T_{s2} of the intermediate compound and the solid solution are higher than other binary system.

Acknowledgements

References

1 J. Fenrych, E. C. Reynhardt, S. Jurga and K. Jurga, Mol. Phys., 78 (1993) 1117.
2 H. R. C. Ouriques, M. F. S. Trindade, M. M. Conceicao, S. Prasad, P. F. A. Filho and A. G. Souza, J. Therm. Anal. Cal., 75 (2004) 569.
3 N. V. Venkataraman, S. Barman and S. Vasudevan, Chem. Phys. Lett., 358 (2002) 139.
4 I. G. Vasilyeva, R. E. Nikolaev, V. V. Malakhov and L. I. Isaenko, J. Therm. Anal. Cal., 90 (2007) 601.
5 F. Querniard, J. Linol, Y. Cartigny and G. Coquerel, J. Therm. Anal. Cal., 90 (2007) 359
6 Y. Tabuchi, K. Asai and M. Rikukawa, J. Phys. Chem. Solids., 61 (2000) 837.

Fig. 4 The binary phase diagram of $C_{10}Mn–C_{14}Mn$

7 A. Terreros, P. A. Galera-Gómez and E. Lopez-Cabarcos, J. Therm. Anal Cal., 61 (2000) 341.

8 K. Z. Wu, C. X. Zhang, Y. J. Li and X. D. Liu, J. Chin. Chem. Soc., 52 (2005) 45.

9 K. Z. Wu, P. Zuo, X. D. Liu and Y. J. Li, Thermochim. Acta, 397 (2003) 49.

10 D. S. Ruan, W. P. Li, L. F. He and Q. H. Hu, J. Thermal Anal., 45 (1995) 235.

11 K. Z. Wu, X. D. Wang and X. D. Liu, J. Univ. Sci. Technol. Beijing, 10 (2003) 75.

12 W. P. Li, D. S. Zhang, T. P. Zhang, T. Z. Wang, D. S. Ruan, D. Q. Xing and H. B. Li, Thermochim. Acta, 326 (1999) 183.

13 V. Salerno, A. Grieco and M. Vacatello, J. Phys. Chem., 80 (1976) 2444.

14 K. Z. Wu, W. Z. Cui and J. J. Zhang, Thermochim. Acta, 463 (2007) 15.

15 R. Courchinoux, N. B. Chanh and Y. Haget, Thermochim. Acta, 128 (1988) 45.

16 P. W. Atkins, Physical Chemistry, Oxford University, Oxford 1990.

17 G. Dravecz, B. Shackmann, M. Cochez and M. Ferriol, J. Therm. Anal. Cal., 90 (2007) 343.

18 E. Wenda and A. Bielański, J. Therm. Anal. Cal., 92 (2008) 921.

19 A. Blonska-Tabero, J. Therm. Anal. Cal., 88 (2007) 201.